Development of a mini-replicon-based reverse-genetics system for rice stripe tenuivirus

Mingfeng Feng[1], Luyao Li[1], Ruixiang Cheng[1], Yulong Yuan[1], Yongxin Dong[1], Minglong Chen[1], Rong Guo[1], Min Yao[1], Yi Xu[1], Yijun Zhou[2], Jianxiang Wu[3], Xin Shun Ding[1], Xueping Zhou[3, 4, *], and Xiaorong Tao[1, *]

[1] Key Laboratory of Plant Immunity, Department of Plant Pathology, College of Plant Protection, Nanjing Agricultural University, Nanjing 210095, P. R. China.

[2] Institute of Plant Protection, Jiangsu Academy of Agricultural Sciences, Jiangsu Technical Service Center of Diagnosis and Detection for Plant Virus Diseases, Nanjing 210014, P.R. China

[3] State Key Laboratory of Rice Biology, Institute of Biotechnology, Zhejiang University, Hangzhou 310029, P. R. China

[4] State Key Laboratory for Biology of Plant Diseases and Insect Pests, Institute of Plant Protection, Chinese Academy of Agricultural Sciences, Beijing 100193, P. R. China

*For Correspondence:

Xiaorong Tao (taoxiaorong@njau.edu.cn); Xueping Zhou (zzhou@zju.edu.cn)

Running Title

A mini-replicon-based reverse-genetics system for RSV

ABSTRACT

Negative-stranded RNA (NSR) viruses include both animal- and plant-infecting viruses that often cause serious diseases in human and livestock, and in agronomic crops. Rice stripe tenuivirus (RSV), a plant NSR virus with four negative-stranded/ambisense RNA segments, is one of the most destructive rice pathogens in many Asian countries. Due to the lack of a reliable reverse-genetics technology, molecular studies of RSV gene functions and its interaction with host plants are severely hampered. To overcome this obstacle, we developed a mini-replicon-based reverse-genetics system for RSV gene functional analysis in *Nicotiana benthamiana*. We first developed a mini-replicon system expressing RSV genomic RNA3 eGFP reporter ($MR3_{(-)eGFP}$), a nucleocapsid (NP), and a codon usage optimized RNA-dependent RNA polymerase ($RdRp_{opt}$), respectively. Using this mini-replicon system we determined that RSV NP and $RdRp_{opt}$ are indispensable for the eGFP expression from $MR3_{(-)eGFP}$. The expression of eGFP from $MR3_{(-)eGFP}$ can be significantly enhanced in the presence of NSs and P19-HcPro-γb. In addition, NSvc4, the movement protein of RSV, facilitated eGFP trafficking between cells. We also developed an antigenomic RNA3-based replicon in *N. benthamiana*. However, we found that the RSV *NS3* coding sequence acts as a *cis*-element to regulate viral RNA expression. Finally, we made mini-replicons representing all four RSV genomic RNAs. This is the first mini-replicon-based reverse-genetics system for monocot-infecting tenuivirus. We believe that this mini-replicon system described here will allow the studies of RSV replication, transcription, cell-to-cell movement

and host machinery underpinning RSV infection in plants.

KEY WORDS: *Rice stripe tenuivirus*, reverse-genetics system, mini-replicon, negative-sense/ambisense RNA virus

IMPORTANCE

Plant-infecting segmented negative-stranded RNA (NSR) viruses are grouped into 3 genera: *Orthotospovirus*, *Tenuivirus* and *Emaravirus*. The reverse-genetics systems have been established for members in the genera *Orthotospovirus* and *Emaravirus*, respectively. However, there is still no reverse-genetics system available for *Tenuivirus*. Rice stripe virus (RSV) is a monocot-infecting tenuivirus with four negative-stranded/ambisense RNA segments. It is one of the most destructive rice pathogens and causes significant damages to rice industry in Asian countries. Due to the lack of a reliable reverse-genetics system, molecular characterizations of RSV gene functions and the host machinery underpinning RSV infection in plants are extremely difficult. To overcome this obstacle, we developed a mini-replicon-based reverse-genetics system for RSV in *Nicotiana benthamiana*. This is the first mini-replicon-based reverse-genetics system for tenuivirus. We consider that this system will provide researchers a new working platform to elucidate the molecular mechanisms dictating segmented tenuivirus infections in plant.

Introduction

Negative-sense RNA (NSR) viruses include well-known members of medical importance such as Ebola virus (EBOV), vesicular stomatitis virus (VSV), influenza A virus (FLUAV) and Rift Valley fever virus (RVFV) (1, 2) and include serious plant pathogens of agrinomical importance such as Tomato spotted wilt virus (TSWV), Rice stripe virus (RSV), and Rose rosette virus (RRV) (3-5). There are 3 genera of segmented NSR viruses infecting plants: *Orthotospovirus, Tenuivirus* and *Emaravirus*. TSWV and RSV are the representative viruses for *Orthotospovirus and Tenuivirus*, respectively (6, 7). RRV and *European mountain ash ringspot-associated virus* (EMAraV) are important members in the genus *Emaravirus* (8, 9).

Tenuiviruses are classified in the genus *Tenuivirus*, family *Phenuiviridae* within the order *Bunyavirales*. Most viruses in the family *Phenuiviridae* infect animals. RSV is one of most devastating causal agents of rice and often causes severe damages to rice production in China and many other Asian countries (6, 10, 11). RSV is transmitted by small brown planthopper (*Laodelphax striatellus*) in a persistent and circulative-propagative manner (6, 12-14). RSV genome consists of four RNA segments and encodes seven proteins through an antisense or an ambisense coding strategy (15-18). RSV RNA1 is of negative polarity and encodes the RNA-dependent RNA polymerase (RdRp) (17). RSV RNA2 encodes the NS2 protein in the viral (v) strand and the NSvc2 protein from the viral complementary (vc) strand (19). The NS2 protein is a weak viral suppressor of RNA silencing (VSR) and is required for RSV systemic infection in plants. The NSvc2 protein is a putative glycoprotein that targets

endoplasmic reticulum (ER) and Golgi apparatus, and function as a helper factor to conquer insect midgut barriers after being cleaved into two mature proteins (i.e., NSvc2-N, the amino-terminal half, and NSvc2-C, the carboxyl-terminal half) (12, 20). RSV RNA3 encodes the NS3 protein in the v strand, and is known as a VSR that binds single- and double-stranded RNAs to suppress RNA silencing (21, 22), and the NP protein in the vc strand that interacts with viral genomic RNAs to form viral ribonucleoprotein complexes (RNPs) (23). RSV RNA4 encodes the SP protein in the v strand, a nonstructural and disease-specific protein that interacts with a host oxygen-evolving complex protein to interfere host photosynthesis, and the NSvc4 protein in the vc strand, a protein involved in RSV cell-to-cell and long-distance movement in plant (4, 21). The four RSV genomic RNAs all contain highly conserved 5′- and 3′-untranslated regions (UTR), important for the initiation of viral RNA transcriptions. RSV RNA2, 3 and 4 all have a noncoding intergenic region (IGR) with multiple AU-rich regions that form secondary hairpin-like structures to act as transcription termination signals (24, 25).

Viral reverse-genetics systems are important tools for the studies of viral gene functions, disease inductions and host factors involved in virus infection in plants (26-32). Although reverse-genetics systems have been firstly reported for animal segmented negative-stranded RNA viruses over 20 years ago (26, 33-43), to establish similar systems for plant segmented negative-stranded/ambisense RNA viruses turned out to be very challenging. However, just recently the reverse-genetics systems have been established for a few of non-segmented and segmented plant NSR viruses. The

first reverse-genetics system of the non-segmented plant NSR viruses was established for *Sonchus yellow net virus* (SYNV, a nucleorhabdovirus) and followed with BYSMV (a cytorhabdovirus) (27, 44-47). Recently we established the first reverse-genetics system of segmented plant NSR viruses for TSWV (48). Soon after, the reverse-genetics system for RRV was also established, allowing for studies of emaravirus gene function and disease pathology in whole plants (9).

For 3 genera of segmented NSR viruses infecting plants, reverse-genetics model has been established for 2 of the genera, *Orthotospovirus* and *Emaravirus* (9, 48, 49). However, there is still no reverse-genetics system available for the genus *Tenuivirus*. The recent progresses on TSWV and RRV reverse-genetics system encouraged us to establish a reverse-genetics system for RSV. In this study, we developed a mini-replicon-based reverse-genetics system for RSV gene function analyses in *Nicotiana benthamiana*. This represents the first mini-replicon-based reverse-genetics system for monocot-infecting tenuivirus. The developed mini-replicon reverse-genetics system will provide researchers a novel platform for studies of RSV replication, transcription, movement and host factors involved in the interactions between the virus and the host plant. This system also provides useful basis for the development of infectious RSV clones for the assays in plants, including rice.

Results

Development of a genomic RNA3 mini-replicon-based reverse-genetics system for RSV

To establish a mini-replicon-based reverse-genetics system to investigate RSV infection in plant, we RT-PCR-amplified the full-length RSV RNA3 sequence and inserted it between an HH sequence and an RZ sequence in the pCB301-2×35S-RZ-NOS vector to produce $RNA3_{(-)}$. We then replaced the *NP* gene in $RNA3_{(-)}$ with an *eGFP* gene to produce $MR3_{(-)eGFP}$ mini-replicon reporter (Fig. 1A). The expressions of $RNA3_{(-)}$ and $MR3_{(-)eGFP}$ from these two vectors are driven by a doubled *Cauliflower mosaic virus* (CaMV) 35S promoter (2×35S) (Fig. 1A).

We constructed p2300-$RdRp_{wt}$, pBIN-NS3, p2300-NP, and pCXSN-NSvc4 to express the wild-type RSV RdRp ($RdRp_{wt}$), NS3, NP, and NSvc4, respectively, in cells through agro-infiltration. After infiltration of a mixed Agrobacterium culture carrying the plasmids of $MR3_{(-)eGFP}$, $RdRp_{wt}$, NP and four VSRs (NSs and P19-HcPro-γb) into *N. benthamiana* leaves (Fig 1B), no eGEP fluorescence was observed in the infiltrated leaves by 5 days post agro-infiltration (dpi) (Fig. 1C). As reported for TSWV RdRp (48), the wild-type RSV RdRp was also predicted to have numerous putative intron splicing sites. This prediction prompted us to optimize its codon usage and to remove the predicted intron splicing sites. The optimized *RdRp* ORF was then inserted into the p2300 vector to produce p2300-$RdRp_{opt}$ ($RdRp_{opt}$). After infiltrating *N. benthamiana* leaves with a mixed Agrobacterium culture carrying plasmids of $MR3_{(-)eGFP}$, $RdRp_{opt}$, NP and four VSRs, we observed the eGFP

fluorescence using a microscope at 5 dpi (Fig. 1B), suggesting that the sequence optimized $RdRp_{opt}$ is now functional in *N. benthamiana* cells.

RSV NP and $RdRp_{opt}$ are required for $MR3_{(-)eGFP}$ expression

To investigate the roles of NP and $RdRp_{opt}$ in RSV replication in plant, we co-expressed $MR3_{(-)eGFP}$ and VSRs with empty vector (Vec), NP, $RdRp_{opt}$, or both NP and $RdRp_{opt}$, respectively, in *N. benthamiana* leaves through agro-infiltration. The eGFP fluorescence was again detected in the leaves co-expressing $MR3_{(-)eGFP}$ with NP and $RdRp_{opt}$. In contrast, the control leaves expressing $MR3_{(-)eGFP}$ alone, or co-expressing $MR3_{(-)eGFP}$ with NP or $RdRp_{opt}$, did not show any eGFP fluorescence (Fig. 2A), indicating that the presence of both NP and $RdRp_{opt}$ is necessary for $MR3_{(-)eGFP}$ expression from the mini-replicon.

To confirm this observation, we analyzed the accumulation levels of eGFP protein, *eGFP* mRNA, and $MR3_{(-)eGFP}$ genomic RNA (gRNA) and anti-genomic RNA (agRNA) in the infiltrated *N. benthamiana* leaf tissues. Western blot showed high levels of eGFP in the leaves co-expressing $MR3_{(-)eGFP}$, NP, $RdRp_{opt}$ and four VSRs (NSs+P19-HcPro-γb). In contrast, eGFP protein was not detected in the control leaves co-expressing $MR3_{(-)eGFP}$ with Vec, NP or $RdRp_{opt}$ only by 5 dpi (Fig. 2B). Northern blot results showed that the gRNA and agRNA were detected in the leaf tissues co-expressing $MR3_{(-)eGFP}$, NP, $RdRp_{opt}$ and VSRs by 5 dpi (Fig. 2C). In contrast, no amplified gRNA and agRNA were detected in the control leaves co-expressing $MR3_{(-)eGFP}$ with Vec, NP or RdRp only, respectively (Fig. 2C). Only primary

174 transcripts of agRNA from $MR3_{(-)eGFP}$ was detected in these leaves. These results
175 indicate that the presence of RSV NP and $RdRp_{opt}$ are required for the replication of
176 both gRNA and agRNA from the $MR3_{(-)eGFP}$ mini-replicon. Intrinsically, the *eGFP*
177 mRNA was not detected in the leaf tissues co-expressing $MR3_{(-)eGFP}$, NP , $RdRp_{opt}$ and
178 VSRs.
179
180 **Effect of viral suppressors of RNA silencing on $MR3_{(-)eGFP}$ expression**
181 Viral suppressors of RNA silencing (VSRs) inhibit host RNAi machinery and enhance
182 non-viral gene expressions in plants (44, 46). To investigate the roles of different
183 VSRs on $MR3_{(-)eGFP}$ expression in plant, we infiltrated *N. benthamiana* leaves with
184 mixed agrobacterium cultures carrying $MR3_{(-)eGFP}$, $RdRp_{opt}$, NP and VSRs including
185 NS3, NSs, and P19-HcPro-γb, respectively. By 5 dpi, the leaves co-expressing
186 $MR3_{(-)eGFP}$, $RdRp_{opt}$ and NP with Vec showed a few cells with eGFP fluorescence.
187 Many cells with eGFP fluorescence were observed in the leaves co-expressing
188 $MR3_{(-)eGFP}$, $RdRp_{opt}$ and NP with three VSRs (P19-HcPro-γb) or four VSRs (NSs
189 and P19-HcPro-γb) (Fig. 3A and 3B). Although RSV NS3 is a VSR (21, 22),
190 co-expression of $MR3_{(-)eGFP}$, $RdRp_{opt}$, NP with NS3 or both NS3 and NSs resulted in
191 almost no cell with eGFP fluorescence. Moreover, co-expression of $MR3_{(-)eGFP}$,
192 $RdRp_{opt}$, NP with both NS3 and P19-HcPro-γb resulted in some cells with eGFP
193 fluorescence. These findings indicate that RSV NS3 can suppress eGFP expression
194 from the $MR3_{(-)eGFP}$ mini-replicon, and are supported by the Western blot result (Fig.
195 3B). Based on these results, we decided to use VSRs including NSs, P19, HcPro and

196 γb but not NS3 in the following experiments.

197

198 **Dosage effects of NP and $RdRp_{opt}$ on $MR3_{(-)eGFP}$ expression**

199 To optimize the expression of $MR3_{(-)eGFP}$ mini-replicon in plant cells, we mixed the
200 Agrobacterium culture carrying $MR3_{(-)eGFP}$ and four VSRs (NSs+P19-HcPro-γb) with
201 the Agrobacterium cultures carrying NP (OD_{600} 0, 0.05, 0.1, 0.2 or 0.4) or $RdRp_{opt}$
202 (OD_{600} 0, 0.05, 0.1, 0.2 or 0.4), and then infiltrated them individually into *N.*
203 *benthamiana* leaves. When the concentration of Agrobacterium culture carrying RdRp
204 was fixed at OD_{600} 0.05 and the concentration of Agrobacterium culture carrying NP
205 was increased from OD_{600} 0.05 to OD_{600} 0.4, the results showed that the strongest
206 eGFP fluorescence was observed in the leaves co-expressing $MR3_{(-)eGFP}$ with NP at
207 OD_{600} 0.2 and $RdRp_{opt}$ at OD_{600} 0.05 (Fig. 4A). When the concentration of
208 Agrobacterium culture carrying NP was maintained at OD_{600} 0.2, while the
209 concentration of Agrobacterium culture carrying $RdRp_{opt}$ was increased from OD_{600}
210 0.05 to OD_{600} 0.4, the number of cells with eGFP fluorescence decreased as the
211 concentration of $RdRp_{opt}$ increased (Fig. 4B). These results were supported by the
212 results from Western blot assays (Fig. 4C and 4D).

213

214 **RSV NSvc4 supports $MR3_{(-)eGFP}$ cell-to-cell movement**

215 NSvc4 is the movement protein of RSV (18, 50). To investigate whether NSvc4 can
216 also influence $MR3_{(-)eGFP}$ expression, we infiltrated *N. benthamiana* leaves with the
217 mixed Agrobacterium cultures carrying $MR3_{(-)eGFP}$ (OD_{600} 0.2), NP (OD_{600} 0.2),

RdRp$_{opt}$ (OD_{600} 0.05), NSs (OD_{600} 0.05), P19-HcPro-γb (OD_{600} 0.05) and NSvc4 (OD_{600} 0.025, 0.05, 0.1 or 0.15). In this experiment, the MR3$_{(-)eGFP}$ started to move out the original cell in the addition of NSvc4 at OD_{600} 0.025, compared with that in the leaves co-expressing MR3$_{(-)eGFP}$, NP and RdRp$_{opt}$ without NSvc4 (Fig. 5A and Table 1). When the concentration of Agrobacterium culture carrying NSvc4 was further increased, stronger cell-to-cell movement of MR3$_{(-)eGFP}$ was observed (Fig. 5A and Table 1). Results of the Western blot assays agreed with the microscopic observations (Fig. 5B).

Development of an RSV antigenomic RNA3-based replicon system

To develop an RSV antigenomic (ag) RNA-based mini-replicon, we replaced the *NS3* gene in the RNA3$_{(+)}$-agRNA vector (RNA3$_{(+)}$) with an *eGFP* gene to produce MR3$_{(+)eGFP}$ (Fig. 6A). We then transiently co-expressed MR3$_{(+)eGFP}$, NP, RdRp$_{opt}$, and four VSRs (NSs+P19-HcPro-γb) in *N. benthamiana* leaves through agro-infiltration. By 5 dpi, no eGFP fluorescence was observed in the infiltrated leaves. In contrast, strong eGFP fluorescence was observed in the leaves co-expressing MR3$_{(-)eGFP}$, NP, RdRp$_{opt}$ and four VSRs (Fig. 6B), indicating that the MR3$_{(+)eGFP}$ min-replicon is incapable of expressing eGFP in plant cells.

Next, we replaced the *NS3* gene in MR3$_{(-)eGFP}$ with a *mCherry* gene (MR3$_{(-)mCherry\&eGFP}$) (Fig. 6C), and co-expressed MR3$_{(-)mCherry\&eGFP}$ or MR3$_{(-)eGFP}$ with NP, RdRp$_{opt}$ and four VSRs in *N. benthamiana* leaves through agro-infiltration. By 5 dpi, in contrast to the leaves co-expressing MR3$_{(-)eGFP}$, NP, RdRp$_{opt}$ and VSRs , no

eGFP fluorescence was observed for $MR3_{(-)mCherry\&eGFP}$ (Fig. 6D), indicating that without the *NS3* gene, this $MR3_{(-)mCherry\&eGFP}$ min-replicon is unable to express eGFP in *N. benthamiana* leaf cells. To confirm this result, we generated $RNA3_{(+)}$ to express full-length RSV agRNA3 (Fig. 6A), and transiently co-expressed $RNA3_{(+)}$, VSRs, NSvc4 with one or two of the three plasmids (i.e., Vec, NP and $RdRp_{opt}$), respectively in *N. benthamiana* leaves via agro-infiltration. The infiltrated leaves were harvested at 5 dpi and analyzed for the accumulations of $RNA3_{(+)}$-derived gRNA3 and agRNA3 through Northern blot assays using DIG labelled antisense- and sense-probes, respectively. The result showed that high levels of gRNA3 and agRNA3 were detected in the leaves co-expressing $RNA3_{(+)}$, NP, $RdRp_{opt}$, VSRs and NSvc4 (Fig. 6E). In contrast, No amplified gRNA3 and agRNA3were detected in the leaves co-expressing $RNA3_{(+)}$, four VSRs, NSvc4 with Vec, NP or $RdRp_{opt}$ only) (Fig. 6E). Only primary transcripts of agRNA3 from $RNA3_{(+)}$ was detected in these leaves. Based on these results, we conclude that the $RNA3_{(+)}$ replicon is functional in *N. benthamiana* in the presence of NP, $RdRp_{opt}$, NSs, P19-HcPro-γb and NSvc4.

The *NS3* gene is required for *eGFP* expression from $MR3_{(-)eGFP}$

To investigate the function of *NS3* in eGFP expression from the $MR3_{(-)eGFP}$ mini-replicon, we introduced a stop codon (TAA) at the downstream of the start codon of *NS3* ORF ($MR3_{(-)eGFP\&NS3stop}$) (Fig. 7A), and co-expressed it with NP, $RdRp_{opt}$ and VSRs in *N. benthamiana* leaves through agroinfiltration. By 5 dpi, strong eGFP fluorescence was observed in the infiltrated leaves, while the leaves

co-expressing $MR3_{(-)eGFP\Delta NS3}$, NP, $RdRp_{opt}$ and VSRs did not (Fig. 7B). Western blot results showed that the eGFP were expressed in the leaves co-expressing $MR3_{(-)eGFP\&NS3stop}$, NP, $RdRp_{opt}$ and VSRs, while no eGFP was accumulated in the leaves co-expressing $MR3_{(-)eGFP\Delta NS3}$, NP, $RdRp_{opt}$ and VSRs (Fig. 7C). This finding indicates that the NS3 is dispensable for eGFP expression from the $MR3_{(-)eGFP}$ mini-replicon. Deletion of *NS3* gene sequence from $MR3_{(-)eGFP}$ ($MR3_{(-)eGFP\Delta NS3}$) abolished the expression of eGFP.

To further confirm the role of *NS3* ORF in $MR3_{(-)eGFP}$ expression, we divided *NS3* ORF into four segments and generated four truncated $MR3_{(-)eGFP}$ mutant constructs: $MR3_{(-)eGFPMut1}$, $MR3_{(-)eGFPMut2}$, $MR3_{(-)eGFPMut3}$, and $MR3_{(-)eGFPMut4}$ (Fig. 7D). Each mutant was co-expressed with NP, $RdRp_{opt}$, NSvc4 and VSRs, respectively, in *N. benthamiana* leaves. By 5 dpi, eGFP fluorescence was observed in the leaves co-expressing $MR3_{(-)eGFPMut2}$, $MR3_{(-)eGFPMut3}$, or $MR3_{(-)eGFPMut4}$ with NP, $RdRp_{opt}$, NSvc4 and VSRs. However, the leaves co-expressing $MR3_{(-)eGFPMut1}$, NP, $RdRp_{opt}$, NSvc4 and VSRs did not show eGFP fluorescence (Fig. 7E). Western blot results agreed with the microscopic observations and showed that eGFP was not expressed from $MR3_{(-)eGFPMut1}$ in cells (Fig. 7F), indicating that deletion of the first 159 aa residues of NS3 significantly affect $MR3_{(-)eGFP}$ mini-replicon to express the eGFP. It is noteworthy that the Northern blot result showed that the expression of gRNA and agRNA from $MR3_{(-)eGFPMut1}$ was not affected (Fig. 7G). We also noticed that the mobility of gRNA and agRNA from $MR3_{(-)eGFPMut2}$ and $MR3_{(-)eGFPMut4}$ was altered compared with that from $MR3_{(-)eGFPMut1}$, $MR3_{(-)eGFPMut3}$ or $MR3_{(-)eGFP}$. Therefore, we

conclude that the *NS3* ORF sequence is not necessary for viral replication but is required for the expression of eGFP from the $RNA3_{(-)}$-derived mini-replicons in cells.

RSV RNA2, 3 and 4 IGRs can form secondary hairpin-like structures which is postulated to act as transcription termination signals (24, 25). To further investigate the possible role of RSV NS3 in viral transcription regulation, we predicted the RNA secondary structure and examined the possible RNA-RNA interaction between NS3 coding sequence, IGR and 3′-UTR of RSV RNA3. The 3′-UTR, NS3, and IGR of RSV RNA3 have 65, 636 and 742 nucleotides (nt), respectively. The secondary structure analysis showed that the1-295 nt sequence of IGR formed a very long hairpin structure (Fig. 8). Strikingly, the 1-40 nt coding region sequence of NS3 base-paired with the 575-596 nt sequence of IGR and the 1-65 nt sequence of 3′-UTR and formed a long hairpin structure (Fig. 8). The 619-636 nt coding region sequence of NS3 base-paired with the 396-403 nt and the 537-543 nt sequences of IGR and formed a small hairpin-like structure. The 41-203 nt coding region sequence of NS3 itself formed four long and short hairpin structures. The 205-618 nt coding region sequence of NS3 formed sector structure containing at least 9 hairpins (Fig. 8). The secondary structure analysis suggested that the coding sequence of NS3 likely interacts with IGR and 3′-UTR of RNA3 in forming hairpin-like structure.

Development of RSV RNA1, RNA2 and RNA4 mini-replicons

RSV genome consists of four RNA segments encoding seven proteins using an antisense or an ambisense coding strategy (15-18). Because the $MR3_{(-)eGFP}$

306 mini-replicon is functional in *N. benthamiana* leaf cells (Fig. 1 and Fig. 2), we
307 decided to develop mini-replicons for other three RSV genomic RNAs. We first
308 produced $MR1_{(-)eGFP}$ and then replaced the *RdRp* ORF with the *eGFP* gene to produce
309 $MR1_{(-)eGFP}$ (Fig. 9A). For RSV genomic RNA2 and 4, we first cloned the full-length
310 RNA2 or 4 segments individually into the vector, and then replaced the *NSvc2* ORF
311 with the *eGFP* gene to produce $MR2_{(-)eGFP}$ or replaced the *NSvc4* ORF with the *eGFP*
312 gene to produce $MR4_{(-)eGFP}$ (Fig. 9A). *N. benthamiana* leaves were then infiltrated
313 with the mixed Agrobacterium cultures carrying various combinations of plasmids
314 (Fig. 9B). By 5 dpi, strong eGFP fluorescence was observed in the leaves
315 co-expressing $MR1_{(-)eGFP}$, $MR2_{(-)eGFP}$, or $MR4_{(-)eGFP}$ with NP, $RdRp_{opt}$ and four VSRs
316 (Fig. 9B). As expected, the leaves infiltrated with the mixed Agrobacterium cultures
317 lacking NP, $RdRp_{opt}$ or NP+$RdRp_{opt}$ did not show eGFP fluorescence.

318 Collectively, the mini-replicon-based reverse-genetics system, representing all
319 four RSV genomic RNAs, has been created.

320

321 **Discussion**

322 There are 3 genera of segmented NSR viruses infecting plants: *Orthotospovirus*,
323 *Tenuivirus* and *Emaravirus*. The reverse-genetics systems have been established for
324 TSWV and RRV in the genera *Orthotospovirus* and *Emaravirus* (9, 48, 49),
325 respectively. Here, we established a mini-replicon-based reverse-genetics system for
326 RSV, the representative virus for the genus *Tenuivirus*. RSV is an important rice virus
327 and poses significant threat to rice productions in China and many other Asian
328 countries (6, 10, 11). During the past 20 years, the lack of a reliable reverse-genetics

329 system significantly hampered the studies of RSV gene functions and disease
330 induction in plant. To overcome this obstacle, we launched a multiyear research that
331 finally yielded a functional mini-replicon-based reversed genetics system for RSV
332 studies. We first developed a mini-replicon system to express RSV $MR3_{(-)eGFP}$, NP,
333 and a codon usage optimized RdRp ($RdRp_{opt}$), respectively. Using this mini-replicon
334 systems we determined that RSV NP and $RdRp_{opt}$ are indispensable for the eGFP
335 expression from $MR3_{(-)eGFP}$. The expression of eGFP from $MR3_{(-)eGFP}$ was
336 significantly enhanced in the presence of NSs and P19-HcPro-γb. In addition, NSvc4,
337 the movement protein of RSV, facilitated eGFP trafficking between cells. Interestingly,
338 co-expression of RSV NS3 inhibited eGFP expression from $MR3_{(-)eGFP}$. We also found
339 that the RSV *NS3* gene sequence is not necessary for viral replication, but regulates
340 viral RNA expression. The secondary structure analysis showed that the coding
341 sequence of NS3 base-paired with the sequence of IGR and 3′-UTR of RNA3 to form
342 a long hairpin structure. The phenomenon of coding sequence as a *cis*-element in
343 regulating viral RNA expression has not been reported previously for the
344 negative-stranded/ambisense RNA viruses. Finally, based on the system of $RNA3_{(-)}$,
345 we have also produced mini-replicons representing all RSV RNA genomic segments,
346 allowing RSV functional studies in plant.

347 The choice of promoter for RNA transcriptions is critical for the development of
348 reverse-genetics systems for plant NSR viruses. The genomic and antigenomic RNAs
349 generated from the negative-stranded RNA virus clones were not infectious because
350 their infectious ribonucleoprotein complexes (RNPs) contain not only viral gRNA,

but also NP and RdRp proteins (36, 51). Genomic RNAs of the same segmented NSV contain highly conserved 5′ and 3′ terminal untranslated sequences that have eight complementary nucleotides, capable of forming panhandle-like structures. These structures are known to play critical roles in viral gRNA and agRNA replications (51). Moreover, the NSR viruses RNAs do not possess 5′ cap-structures and 3′ poly(A) tails. The classical bacteriophage T7 promoter can produce accurate viral RNA 5′ end sequences without a cap. We initially produced an RSV mini-replicon systems using the T7 promoter. This mini-replicon system, however, did not express the *eGFP* gene from an RNA3-based mini-replicon in plant cells. In our recent report, we also reported that the T7 promoter-based system was unable to generate infectious TSWV RNA transcripts in plant cells (48). It is possible that the synthesis of viral genomic RNA transcripts through the T7 promoter and T7 RNA polymerase is incomplete or is inefficient in *planta*.

In a recent report, we described an expressing vector with a double CaMV 35S promoter (an RNA Pol II promoter), a hammerhead (HH) ribozyme, and an HDV ribozyme to produce infectious TSWV viral RNAs in plant cells (48). The mini-replicon system produced in this study also has an HH ribozyme and an HDV ribozyme before and after the viral sequence to ensure the correct ends. The results shown in Fig. 1 and Fig. 2 suggest that the vector transcribed RSV genomic RNA did bind to viral NP and RdRp to form functional RNPs, which is needed for the synthesis of functional viral gRNA and agRNA. This finding supports earlier reports that the Pol II promoter can not only replicate non-segmented plant NSR viruses (44, 46), but

373 also segmented plant NSR viruses (9, 48).

374 RSV RdRp is one of the major components needed for the initiation of viral
375 genomic RNA replication (17). RSV RdRp is a 337 kDa protein. When this protein
376 was co-expressed with the mini-replicon in plant cells, no eGFP fluorescence was
377 observed in the infiltrated leaves (Fig. 1A-C). Our computer prediction suggested that
378 the RSV *RdRp* sequence contained many putative cryptic intron splicing sites.
379 Because the segmented plant NSR viruses replicate in cytoplasm, their *RdRp* gene
380 sequences should not been evolved to remove those cryptic intron splicing sites that
381 could be spliced in cell nucleus. We speculated that after the wild-type RSV *RdRp*
382 sequences were expressed, through the 2×35S promoter, in nucleus, they were quickly
383 spliced, resulting in non-functional *RdRp* fragments. After the putative intron splicing
384 sites were removed and the codon usage was optimized, the expressed $RdRp_{opt}$ is
385 capable of supporting *eGFP* expression from the mini-replicon (Fig. 1D). In this study,
386 we also determined that the less concentrated Agrobacterium culture carrying $RdRp_{opt}$
387 (OD_{600} 0.05) caused higher eGFP expression in cells. In contrast, increase of
388 Agrobacterium culture carrying $RdRp_{opt}$ from OD_{600} 0.1 to OD_{600} 0.4 decreased eGFP
389 expression from the mini-replicon (Fig. 4B and 4C), suggesting that an optimum
390 concentration of $RdRp_{opt}$ is required during RSV infection in plant.

391 Analyses of the five different VSRs have indicated that in the presence of NSs or
392 P19-HcPro-γb, the eGFP expression from the mini-replicon was significantly
393 enhanced (Fig. 3B and 3C). These VSRs are known to function at different steps in
394 host RNA interference (RNAi) pathway during virus infection in plant (44, 52).

Consequently, we conclude that these steps in the RNAi pathway can all affect eGFP expression from the mini-replicon. It is noteworthy that the presence of RSV NS3 alone or NS3 plus one or three of the four VSRs (i.e., NSs or P19-HcPro-γb) suppressed eGFP expression from the RNA3 mini-replicon (3B and 3C) suggesting that RSV NS3 is a negative regulator of RSV RNA3 mini-replicon expression. Similar phenomenon was also reported for TSWV NSs during virus rescue assays using cDNA clones (48). We hypothesize that this negative regulation is caused by the co-suppression of *NS3* gene expression. In this study, addition of NSvc4 significantly increased the number of cells with eGFP fluorescence (Fig. 5A and 5B), further conforming its role in cell-to-cell trafficking.

When the *NS3* gene was replaced with a *mCherry* gene ($MR3_{(-)mCherry\&eGFP}$) or with an *eGFP* gene in $MR3_{(+)eGFP}$, no mCherry or eGFP fluorescence was observed in the leaf tissues co-expressing NP, $RdRp_{opt}$ and VSRs (Fig. 6C and 6D). Deletion of the *NS3* gene sequence abolished the function of $MR3_{(-)eGFP}$. However, gRNA and agRNA were detected in the leaves co-expressing $RNA3_{(+)}$, NP, $RdRp_{opt}$, NSvc4 and VSRs (Fig. 6A and 6E). The $MR3_{(-)eGFP\&NS3stop}$ mini-replicon contains a translation stop codon immediately after the start codon of NS3 and is still functional in *N. benthamiana* leaves (Fig. 7A, 7B and 7C). This finding suggests that the *NS3* coding sequence is required for the eGFP expression of the mini-replicon, probably required for viral transcription. Through nucleotide deletion assays, we determined that the region encompassing nt 1-477 in the *NS3* ORF is not sufficient to express eGFP from the $MR3_{(-)eGFP}$ mini-replicon (Fig. 7D, and 7E-G), even though the mutant

mini-replicon ($MR3_{(-)eGFPMut1}$) is capable of expressing RNA in cells, based on the Northern blot results. Because the positions of the gRNA and agRNA bands from $MR_{3(-)eGFPMut2}$ and $MR_{3(-)eGFPMut4}$ were altered, we speculate that the *NS3* ORF sequence may act as a *cis*-regulatory element during RSV RNA3 viral transcription. Importantly, the secondary structure analysis suggested that the coding sequence of NS3 interacts with IGR and 3′-UTR to form a hairpin-like structure and NS3 itself also forms sophisticated hairpin-like structure (Fig 8). Hairpin structure of TSWV and RSV IGR have been shown to regulate viral transcription termination (53). This is consistent with our findings that *NS3* coding sequence involved in regulation of viral RNA transcription. In our earlier studies, deletion of *NSs* coding sequence from the TSWV S-based mini-replicon system had no clear effect on RNA synthesis (48). Although the genome structure of RSV RNA3 is similar to that of TSWV S RNA, this is the first evidence showing that the *NS3* coding region can act as *cis*-element to regulate the synthesis of viral RNA transcripts of plant segmented NSR viruses.

Based the established mini-replicon system for $MR3_{(-)eGFP}$, we have also produced mini-replicons to express $MR1_{(-)eGFP}$, $MR2_{(-)eGFP}$, and $MR4_{(-)eGFP}$ as described in (Fig. 9A). In the presence of NP, $RdRp_{opt}$ and VSRs, eGFP was expressed from $MR1_{(-)eGFP}$, $MR2_{(-)eGFP}$, and $MR4_{(-)eGFP}$ mini-replicons, respectively (Fig. 9B). We also constructed full-length infectious cDNA clones representing RSV genomic RNA1, RNA2 and RNA4. Infiltration of *N. benthamiana* leaves with the mixed Agrobacterium culture carrying $RNA1_{(-)}$, $RNA2_{(-)}$, $RNA3_{(-)}$, $RNA4_{(-)}$and NP+$RdRp_{opt}$+VSRs did not yield a systemic infection. Because *N. benthamiana* is an

experimental host of RSV and the accumulations of RSV RNAs and proteins are lower than that in the rice plants, it is possible that the low level of RSV RNAs and proteins in the infiltrated *N. benthamiana* leaves fails to rescue of RSV systemic infection. It is also possible that the difficulty of delivering four RSV RNA segments into the same cells prevents the systemic infection. We have also infiltrated rice callus tissues with the mixed Agrobacterium culture carrying $MR1_{(-)eGFP}$, $MR2_{(-)eGFP}$, $MR3_{(-)eGFP}$, $MR4_{(-)eGFP}$ and NP+$RdRp_{opt}$+VSRs, none of them work in rice callus tissues.

In conclusion, there are 3 genera of segmented NSR viruses infecting plants and the replicon-based reverse-genetics system has been established for 2 genera. We now established a mini-replicon-based reverse-genetics system for a tenuivirus in *N. benthamiana*. This is the first mini-replicon-based reverse-genetics system for the segmented monocot-infecting tenuivirus, and will provide a useful platform for studies of RSV gene functions during viral replication, cell-to-cell movement and interactions between RSV and host factors in plants. Knowledge learned from this study also benefit the future constructions of full-length multi-segmented infectious clones for tenuivirus in plants.

Materials and Methods

Plant growth and virus source.

Nicotiana benthamiana plants were grown inside a growth chamber maintained at 25°C and a 16/8 h light and dark photoperiod, and used for assays at about 7-leaf

462 stage. RSV was originally isolated from an RSV-infected rice plant as reported (12).
463 Optimization of RSV *RdRp* ORF codon usage and deletion of putative intron splicing
464 sites were performed based on the predictions using the GeneArt^{TM} Project Manager
465 online software (https://www.thermofisher.com/order/geneartgenes/projectm gmt).
466
467 **Plasmid construction**
468 ***Constructions of RSV RdRp, RdRp$_{opt}$, NP, NSvc4, NS3 and VSRs mini-replicons.***
469 Complementary DNAs (cDNAs) of *RSV*, *NP*, *RdRp*, *RdRp$_{opt}$*, *NS3* and *NSvc4* gene
470 were individually amplified from a total RNA sample isolated from an RSV-infected
471 rice plant through reverse transcription polymerase chain reaction (RT-PCR) using
472 gene specific primers. The resulting RT-PCR products were inserted individually into
473 the expression vector pCambia2300 (refers to as p2300 thereafter), pBINplus, or
474 pCXSN to generate p2300-RdRp$_{wt}$, pBIN-NS3, p2300-NP and pCXSN-NSvc4,
475 respectively. The pCXSV-NSs vector was constructed by inserting a NSs fragment
476 amplified from a cDNA from a TSWV-infected *N. benthamiana* plant into the pCXSN
477 vector. Plasmid pCB301-P19-HcPro-γb (P19-HcPro-γb) that can simultaneously
478 expresses the *Tomato bushy stunt virus* P19 protein, the *Tobacco etch virus* HcPro
479 protein, and the *Barley stripe mosaic virus* γb protein is from a previously published
480 source (46). To construct p2300-RdRp$_{opt}$, we first optimized RdRp$_{wt}$ codon usage and
481 deleted the putative intron splicing sites in it at the GenScript Biotech Corp (Nanjing,
482 China) followed by inserting the synthesized sequence into the p2300 vector to
483 produce p2300-RdR$_{opt}$ (RdRp$_{opt}$).
484 ***Constructions of MR3$_{(-)eGFP}$, MR3$_{(-)mCherry\&eGFP}$ and MR3$_{(+)eGFP}$ mini-replicons.*** To

generate the $MR3_{(-)eGFP}$ and the $MR3_{(+)eGFP}$ mini-replicons, we first prepared cDNAs from a total RNA sample isolated from an RSV-infected rice plant using the Reverse Transcription Kit as instructed (Promega, Madison, WI, USA). We then amplify the full-length RSV $RNA3_{(-)}$ and $RNA3_{(+)}$ sequences from this cDNA through PCR using RSV RNA3 specific primers (Table S1) and a Phanta Super-Fidelity DNA Polymerase (Vazyme Biotech, Nanjing, China). Both PCR products contained a hammerhead (HH) ribozyme (54) before the 5′ end, and then cloned individually behind the 2×35S promoter in the pCB301-2×35S-RZ-NOS vector to generate pCB301-2×35S-HH-$RNA3_{(-)}$-RZ-NOS (refers to as $RNA3_{(-)}$) or pCB301-2×35S-HH-$RNA3_{(+)}$-RZ-NOS ($RNA3_{(+)}$). The presence of an HH and a Hepatitis delta virus ribozyme (RZ) in these two vectors allow the productions of $RNA3_{(-)}$ and $RNA3_{(+)}$ with near perfect ends. To produce a $MR3_{(-)eGFP}$ and a $MR3_{(+)eGFP}$ mini-replicon, we first amplified the *eGFP* gene from $SR_{(+)eGFP}$ (48) using primer FMF37 and FMF38, and then used it to replace the *NP* gene in the $RNA3_{(-)}$ and $RNA3_{(+)}$ through *in vitro* homologous recombination using a ClonExpress II One Step Cloning Kit (Vazyme Biotech, Nanjing, China). The resulting plasmids were referred to as $MR3_{(-)eGFP}$ and $MR3_{(+)eGFP}$, respectively. To produce an $MR3_{(-)mCherry\&eGFP}$ min-replicon with both *mCherry* and *eGFP* gene, we PCR-amplified the *mCherry* gene from the TSWV $SR_{(-)mCherry\&eGFP}$ mini-replicon as reported previously (48) using primer FMF267 and FMF269, and used it to replace the *NS3* gene in $MR3_{(-)eGFP}$ through homologous recombination as describe above. All primers used in this study are listed in Table S1.

Constructions of mutant MR3$_{(-)eGFP}$ mini-replicons. To produce these mutant mini-replicons, we first introduced a stop codon (TAA) after the original start codon of the *NS3* gene through PCR using MR3$_{(-)eGFP}$ as the template, and primer FMF528 and FMF36. This NS3stop fragment was then used to replace the *NS3* gene in MR3$_{(-)eGFP}$ through homologous recombination using prime FMF40 and FMF529. The resulting plasmid is named as MR3$_{(-)eGFP\&NS3stop}$. We then deleted a 636 nucleotides (nt) fragment from the *NS3* gene in MR3$_{(-)eGFP}$ through PCR using primer LLY40 and FMF42, and then inserted it into the pCB301 vector through homologous recombination using prime FMF37 and LLY105 to produce MR3$_{(-)eGFP\Delta NS3}$.

To further investigate the role of RSV *NS3* gene in viral RNA replication and transcription from RNA3$_{(-)}$, we divided *NS3* ORF into four fragments and amplified them individually through PCR using specific primers. These four fragments are: nucleotide position 1-159, 160-318, 319-477, and 478-636, respectively. These fragments were then used to generate MR3$_{(-)eGFPMut1}$, MR3$_{(-)eGFPMut2}$, MR3$_{(-)eGFPMut3}$, and MR3$_{(-)eGFPMut4}$, respectively. Primers used in this study are listed in Table S1. The plasmids were transformed individually into *Agrobacterium tumefaciens* strain GV3101 through electroporation, and the transformants are maintained at -80°C until use.

Agrobacterium infiltration

A. tumefaciens culture were prepared as described previously (44, 45). Briefly, agrobacterium cultures carrying specific plasmids were grown individually in a

culture medium and then diluted to OD_{600} = 1.0, or as indicated in the text, in an infiltration buffer (10 mM MES and 10 mM MgCl2, pH 5.6, supplemented with 100 μM acetosyringone). After 2-3 h incubation in the dark and at room temperature (RT), Agrobacterium cultures harboring p2300-NP (OD_{600} = 0.2), p2300-RdRp (OD_{600} = 0.05), p2300-NSs (OD_{600} = 0.1), pCB301-P19-HcPro-γb (OD_{600} = 0.1) or one of the vectors (OD_{600} = 0.2 each) with an *eGFP* and/or an *mCherry* report gene were mixed in equal volumes, or as indicated in the text. The mixed cultures were then infiltrated individually into leaves of 6-7 leaf-stage-old *N. benthamiana* plants using 1 mL needless syringes. The infiltrated plants were grown inside a growth chamber with the same growth conditions as described above.

Western blot assay

The agro-infiltrated *N. benthamiana* leaves were harvested at 5 days post agro-infiltration (dpi) and homogenized (1 mg/sample) individually in 1 mL extraction buffer (150 mM NaCl, 25 mM Tris-HCl, pH 7.5, 1 mM EDTA, 2% polyvinylpolypyrrolidone, 10 mM dithiothreitol, 10% glycerol, 0.5% Triton X-100, and 1× protease inhibitor cocktail reagent). The crude extract from each sample was mixed with a 5□×□loading buffer at a 1:4 ratio (v/v). All the samples were boiled for 10 min and then incubated on ice for 5 min followed by electrophoresis in 12% SDS-PAGE gels. After the protein bands were transferred onto PVDF membranes (GE Healthcare, UK), the blots were probed with an RSV NP specific (1:5000 diluted) or an eGFP specific (1:3000 diluted) antibody followed by a horseradish peroxidase

(HRP)-conjugated goat anti-mouse or anti-rabbit secondary antibody (1:10000 diluted). The detection signal was visualized using the ECL Substrate Kit as instructed (Thermo Fisher Scientific, Rockford, USA). The ponceau S-stained Rubisco large subunit gels were used to show sample loadings.

Northern blot assay

To detect the expressions of RSV gRNAs, agRNAs, and *eGFP* mRNA, we isolated total RNA from the agro-infiltrated *N. benthamiana* leaf tissues using the RNAprep Pure Plant Kit (Tiangen Biotech, Beijing, China). The isolated total RNA samples were separated in 1% formaldehyde agarose gels through electrophoresis, and then transferred onto Hybond-N^+ membranes (GE Healthcare, UK) (55). DIG-labeled RNA probes specific for the sense or antisense *eGFP* mRNA were *in vitro* synthesized using the DIG High Prime RNA labeling kit (Roche, Basel, Switzerland). The blotted membranes were probed with DIG-labeled RNA probes specific for the sense or antisense *eGFP* mRNA. The detection signal was visualized using a DIG-High Prime Detection Starter Kit II as instructed (Roche).

Fluorescence microscopy

The agro-infiltrated *N. benthamiana* leaf tissues were harvested at 5 dpi, and examined under an inverted fluorescence microscope (OLYMPUS IX71-F22FL/DIC, Tokyo, Japan) equipped with a green barrier filter. The captured images were processed using the ImagePro system (OLYMPUS, Tokyo, Japan) and then the Adobe

573 Photoshop CS4 (San Jose, CA, USA).

574

575 **Acknowledgments**

576 This work was supported by the National Natural Science Foundation of China
577 (31630062, 31925032 and 31870143), the Fundamental Research Funds for the
578 Central Universities (JCQY201904 and KYXK202012), Youth Science and
579 Technology Innovation Program to XT, Project funded by China Postdoctoral Science
580 Foundation (2020M681643) to MF.

581

582 **Author contributions**

583 M.F., L.L. and X.T. conceived and designed the experiments and M.Y., Y.Z., J.W. and
584 Y.X. provided input. M.F., L.L., R.C., Y.Y., Y.D., M.C., and G.R. performed the
585 experiments. M.F., X.D., X.Z. and X.T. wrote the manuscript.

586

587 **Competing interests:**

588 The authors declare that no competing interests exist.

589

590 **Data availability**

591 All data produced in this study are presented in this manuscript or as the supporting
592 files.

593

594 **References**

595 1. **Fields BN, Knipe, D. M., & Howley, P. M.** 1996. Fields Virology (Lippincott-Raven, New

York).

2. **Elliott RM B, G.** 2011. Molecular Biology of Orthobunyaviruses. In: Plyusnin, A., Elliott, R.M. (Eds.), The Bunyaviridae: Molecular and Cellular Biology. Horizon Scientific Press, Norwhich, UK.
3. **Scholthof KB, Adkins S, Czosnek H, Palukaitis P, Jacquot E, Hohn T, Hohn B, Saunders K, Candresse T, Ahlquist P, Hemenway C, Foster GD.** 2011. Top 10 plant viruses in molecular plant pathology. Mol Plant Pathol **12:**938-954.
4. **Kong LF, Wu JX, Lu LN, Xu Y, Zhou XP.** 2014. Interaction between Rice stripe virus disease-specific protein and host PsbP enhances virus symptoms. Mol Plant **7:**691-708.
5. **Laney AG, Keller KE, Martin RR, Tzanetakis IE.** 2011. A discovery 70 years in the making: characterization of the Rose rosette virus. J Gen Virol **92:**1727-1732.
6. **Falk BW, Tsai JH.** 1998. Biology and molecular biology of viruses in the genus Tenuivirus. Annu Rev Phytopathol **36:**139-163.
7. **Zhu M, Jiang L, Bai BH, Zhao WY, Chen XJ, Li J, Liu Y, Chen ZQ, Wang BT, Wang CL, Wu Q, Shen QH, Dinesh-Kumar SP, Tao XR.** 2017. The intracellular immune receptor Sw-5b confers broad-spectrum resistance to tospoviruses through recognition of a conserved 21-amino acid viral effector epitope. Plant Cell **29:**2214-2232.
8. **Mielke N, Muehlbach HP.** 2007. A novel, multipartite, negative-strand RNA virus is associated with the ringspot disease of European mountain ash (Sorbus aucuparia L.). J Gen Virol **88:**1337-1346.
9. **Verchot J, Herath V, Urrutia CD, Gayral M, Lyle K, Shires MK, Ong K, Byrne D.** 2020. Development of a reverse genetic system for studying rose rosette virus in whole plants. Mol Plant Microbe Interact **33:**1209-1221.
10. **Otuka A, Matsumura M, Sanada-Morimura S, Takeuchi H, Watanabe T, Ohtsu R, Inoue H.** 2010. The 2008 overseas mass migration of the small brown planthopper, Laodelphax striatellus, and subsequent outbreak of rice stripe disease in western Japan. Appl Entomol Zool **45:**259-266.
11. **Wang HD, Chen JP, Zhang HM, Sun XL, Zhu JL, Wang AG, Sheng WX, Adams MJ.** 2008. Recent rice stripe virus epidemics in zhejiang province, China, and experiments on sowing date, disease-yield loss relationships, and seedling susceptibility. Plant Dis **92:**1190-1196.
12. **Lu G, Li S, Zhou CW, Qian X, Xiang Q, Yang TQ, Wu JX, Zhou XP, Zhou YJ, Ding XS, Tao XR.** 2019. Tenuivirus utilizes its glycoprotein as a helper component to overcome insect midgut barriers for its circulative and propagative transmission. PLoS Pathog **15:**e1007655.
13. **Zhao W, Yang PC, Kang L, Cui F.** 2016. Different pathogenicities of Rice stripe virus from the insect vector and from viruliferous plants. New Phytol **210:**196-207.
14. **Toriyama S.** 1986. Rice stripe virus: prototype of a new group of viruses that replicate in plants and insects. Microbiol Sci **3:**347-351.
15. **Zhu Y, Hayakawa T, Toriyama S, Takahashi M.** 1991. Complete nucleotide sequence of RNA 3 of rice stripe virus: an ambisense coding strategy. J Gen Virol **72 (Pt 4):**763-767.
16. **Takahashi M, Toriyama S, Hamamatsu C, Ishihama A.** 1993. Nucleotide sequence and possible ambisense coding strategy of rice stripe virus RNA segment 2. J Gen Virol **74:**769-773.
17. **Toriyama S, Takahashi M, Sano Y, Shimizu T, Ishihama A.** 1994. Nucleotide sequence of

RNA 1, the largest genomic segment of rice stripe virus, the prototype of the tenuiviruses. J Gen Virol **75:**3569-3579.

18. **Xiong RY, Wu JX, Zhou YJ, Zhou XP.** 2008. Identification of a movement protein of the tenuivirus rice stripe virus. J Virol **82:**12304-12311.
19. **Du ZG, Xiao DL, Wu JG, Jia DS, Yuan ZJ, Liu Y, Hu LY, Han Z, Wei TY, Lin QY, Wu ZJ, Xie LH.** 2011. p2 of rice stripe virus (RSV) interacts with OsSGS3 and is a silencing suppressor. Mol Plant Pathol **12:**808-814.
20. **Yao M, Liu XF, Li S, Xu Y, Zhou YJ, Zhou XP, Tao XR.** 2014. Rice stripe tenuivirus NSvc2 glycoproteins targeted to the Golgi body by the n-terminal transmembrane domain and adjacent cytosolic 24 amino acids via the COP I- and COP II-dependent secretion pathway. J Virol **88:**3223-3234.
21. **Xiong RY, Wu JX, Zhou YJ, Zhou XP.** 2009. Characterization and subcellular localization of an RNA silencing suppressor encoded by Rice stripe tenuivirus. Virology **387:**29-40.
22. **Shen M, Xu Y, Jia R, Zhou X, Ye KQ.** 2010. Size-independent and noncooperative recognition of dsRNA by the Rice stripe virus RNA silencing suppressor NS3. J Mol Biol **404:**665-679.
23. **Lu G, Li J, Zhou YJ, Zhou XP, Tao XR.** 2017. Model-based structural and functional characterization of the Rice stripe tenuivirus nucleocapsid protein interacting with viral genomic RNA. Virology **506:**73-83.
24. **Muhlberger E, Lotfering B, Klenk HD, Becker S.** 1998. Three of four nucleocapsid proteins of Marburg virus, NP, VP35, and L, are sufficient to mediate replication and transcription of marburg virus-specific monocistronic minigenomes. J Virol **72:**8756-8764.
25. **Wu GT, Lu YW, Zheng HM, Lin L, Yan F, Chen JP.** 2013. Transcription of ORFs on RNA2 and RNA4 of Rice stripe virus terminate at an AUCCGGAU sequence that is conserved in the genus Tenuivirus. Virus Res **175:**71-77.
26. **Neumann G, Whitt MA, Kawaoka Y.** 2002. A decade after the generation of a negative-sense RNA virus from cloned cDNA - what have we learned? J Gen Virol **83:**2635-2662.
27. **Jackson AO, Li ZH.** 2016. Developments in plant negative-strand RNA virus reverse genetics. Annu Rev Phytopathol **54:**469-498.
28. **Jackson AO, Dietzgen RG, Goodin MM, Li Z.** 2018. Development of model systems for plant rhabdovirus research. Adv Virus Res **102:**23-57.
29. **Chen YT, Dessau M, Rotenberg D, Rasmussen DA, Whitfield AE.** 2019. Entry of bunyaviruses into plants and vectors. Adv Virus Res **104:**65-96.
30. **Feng MF, Feng ZK, Li ZH; Wang XB, Tao, XB.** 2020. Advances in reverse genetics system of plant negative-strand RNA viruses (in Chinese). Chin Sci Bull **65:**4073-4083.
31. **German TL, Lorenzen MD, Grubbs N, Whitfield AE.** 2020. New technologies for studying negative-strand RNA viruses in plant and arthropod hosts. Mol Plant Microbe Interact **33:**382-393.
32. **Zang Y, Fang XD, Qiao JH, Gao Q, Wang XB.** 2020. Reverse genetics systems of plant negativestrand RNA viruses are difficult to be developed but powerful for virus-host interaction studies and virus-based vector applications. Phytopathology Research **2:**29-37.
33. **Dunn EF, Pritlove DC, Jin H, Elliott RM.** 1995. Transcription of a recombinant bunyavirus rna template by transiently expressed bunyavirus proteins. Virology **211:**133-143.

34. **Bridgen A, Elliott RM.** 1996. Rescue of a segmented negative-strand RNA virus entirely from cloned complementary DNAs. Proc Natl Acad Sci U S A **93:**15400-15404.

35. **Neumann G, Watanabe T, Ito H, Watanabe S, Goto H, Gao P, Hughes M, Perez DR, Donis R, Hoffmann E, Hobom G, Kawaoka Y.** 1999. Generation of influenza A viruses entirely from cloned cDNAs. Proc Natl Acad Sci U S A **96:**9345-9350.

36. **Pekosz A, He B, Lamb RA.** 1999. Reverse genetics of negative-strand RNA viruses: closing the circle. Proc Natl Acad Sci U S A **96:**8804-8806.

37. **Lee KJ, Novella IS, Teng MN, Oldstone MBA, de la Torre JC.** 2000. NP and L proteins of lymphocytic choriomeningitis virus (LCMW) are sufficient for efficient transcription and replication of LCMV genomic RNA analogs. J Virol **74:**3470-3477.

38. **Flick R, Pettersson RF.** 2001. Reverse genetics system for Uukuniemi virus (Bunyaviridae): RNA polymerase I-catalyzed expression of chimeric viral RNAs. J Virol **75:**1643-1655.

39. **Flatz L, Bergthaler A, de la Torre JC, Pinschewer DD.** 2006. Recovery of an arenavirus entirely from RNA polymerase I/II-driven cDNA. Proc Natl Acad Sci U S A **103:**4663-4668.

40. **Luytjes W, Krystal M, Enami M, Parvin JD, Palese P.** 1989. Amplification, expression, and packaging of foreign gene by influenza virus. Cell **59:**1107-1113.

41. **Conzelmann KK, Schnell M.** 1994. Rescue of synthetic genomic RNA analogs of rabies virus by plasmid-encoded proteins. J Virol **68:**713-719.

42. **Volchkov VE, Volchkova VA, Muhlberger E, Kolesnikova LV, Weik M, Dolnik O, Klenk HD.** 2001. Recovery of infectious Ebola virus from complementary DNA: RNA editing of the GP gene and viral cytotoxicity. Science **291:**1965-1969.

43. **Neumann G, Whitt MA, Kawaoka Y.** 2002. A decade after the generation of a negative-sense RNA virus from cloned cDNA - what have we learned? J Gen Virol **83:**2635-2662.

44. **Ganesan U, Bragg JN, Deng M, Marr S, Lee MY, Qian S, Shi M, Kappel J, Peters C, Lee Y, Goodin MM, Dietzgen RG, Li Z, Jackson AO.** 2013. Construction of a sonchus yellow net virus minireplicon: a step toward reverse genetic analysis of plant negative-strand RNA viruses. J Virol **87:**10598-10611.

45. **Wang Q, Ma XL, Qian SS, Zhou X, Sun K, Chen XL, Zhou XP, Jackson AO, Li ZH.** 2015. Rescue of a plant negative-strand RNA virus from cloned cDNA: insights into enveloped plant virus movement and morphogenesis. PLoS Pathog **11:**e1005223.

46. **Fang XD, Yan T, Gao Q, Cao Q, Gao DM, Xu WY, Zhang ZJ, Ding ZH, Wang XB.** 2019. A cytorhabdovirus phosphoprotein forms mobile inclusions trafficked on the actin/ER network for viral RNA synthesis. J Exp Bot **70:**4049-4062.

47. **Gao Q, Xu WY, Yan T, Fang XD, Cao Q, Zhang ZJ, Ding ZH, Wang Y, Wang XB.** 2019. Rescue of a plant cytorhabdovirus as versatile expression platforms for planthopper and cereal genomic studies. New Phytol **223:**2120-2133.

48. **Feng MF, Cheng RX, Chen ML, Guo R, Li LY, Feng ZK, Wu JY, Xie L, Hong J, Zhang ZK, Kormelink R, Tao XR.** 2020. Rescue of tomato spotted wilt virus entirely from complementary DNA clones. Proc Natl Acad Sci U S A **117:**1181-1190.

49. **Ishibashi K, Matsumoto-Yokoyama E, Ishikawa M.** 2017. A tomato spotted wilt virus S RNA-based replicon system in yeast. Sci Rep **7:**12647.

50. **Fu S, Xu Y, Li CY, Li Y, Wu JX, Zhou XP.** 2018. Rice stripe virus interferes with S-acylation of remorin and induces its autophagic degradation to facilitate virus infection. Mol

Plant **11:**269-287.

51. **Ferron F, Weber F, de la Torre JC, Reguera J.** 2017. Transcription and replication mechanisms of Bunyaviridae and Arenaviridae L proteins. Virus Res **234:**118-134.

52. **Burgyan J, Havelda Z.** 2011. Viral suppressors of RNA silencing. Trends Plant Sci **16:**265-272.

53. **van Knippenberg I, Goldbach R, Kormelink R.** 2005. Tomato spotted wilt virus S-segment mRNAs have overlapping 3'-ends containing a predicted stem-loop structure and conserved sequence motif. Virus Res **110:**125-131.

54. **Herold J, Andino R.** 2000. Poliovirus requires a precise 5' end for efficient positive-strand RNA synthesis. J Virol **74:**6394-6400.

55. **Feng MF, Zuo DP, Jiang XZ, Li S, Chen J, Jiang L, Zhou XP, Jiang T.** 2018. Identification of Strawberry vein banding virus encoded P6 as an RNA silencing suppressor. Virology **520:**103-110.

744 **Table 1.** RSV NSvc4 enhances the cell-to-cell movement of $MR3_{(-)eGFP}$
745 mini-replicon in the presence of NP, $RdRp_{opt}$ and four VSRs.

NSvc4[a] OD_{600}	Total eGFP fluorescent cells	No. of clusters with 1 cell (% of total)	No. of clusters with 2 cells (% of total)	No. of clusters with 3≥cells (% of total)
0	18	18 (100%)[b]	0 (100)	0 (100)
0.025	54	15 (27.8%)	6 (22.2%)	5 (50%)
0.05	76	12 (15.8%)	7 (18.4%)	10 (65.8%)
0.1	95	8 (8.4%)	11 (23.2%)	13 (68.4%)
0.15	140	17 (12.1%)	9 (12.9%)	18 (75%)

746 [a] Agrobacterium cultures harboring the plasmid encoding NSvc4 (final concentration,
747 OD_{600} = 0, 0.025, 0.05, 0.1 and 0.15) were used to infiltrate *N. benthamiana* leaves.

748 [b] eGFP fluorescent foci of RSV $MR3_{(-)eGFP}$ at 5 days post-infiltration.

749

750

751

752

753

754

755

756

757

758

759

760

761

762

763

764

765 **Figure legends**

766 **Fig. 1** Construction of an RSV RNA3$_{(-)}$-based mini-replicon. (A) Schematics
767 representing the RdRp$_{wt}$, RdRp$_{opt}$, NP, RSV RNA3$_{(-)}$ and MR3$_{(-)eGFP}$ mini-replicong.
768 For MR3$_{(-)eGFP}$, we replaced the *NP* gene in the gRNA3 with an *eGFP* gene. The 5′
769 untranslated, the 3′ untranslated, and the intergenic region in RNA3$_{(-)}$ were indicated
770 with a thin black line. 2×35S, doubled 35S promoter; HH, hammerhead ribozyme; RZ,
771 hepatitis delta virus (HDV) ribozyme; 35S Ter, 35S terminator; NOS, nopaline
772 synthase terminator. Minus sign (-) and 5′ to 3′ designation represent the viral
773 (genomic)-strand of RNA3. (B) Illustration of agro-infiltration using a mixed
774 Agrobacterium culture carrying various min-replicons into *N. benthamiana* leaves.
775 VSRs, NSs plus P19-HcPro-γb. (C) A *N. benthamiana* leaf infiltrated with a mixed
776 Agrobacterium culture carrying MR3$_{(-)eGFP}$, RdRp$_{wt}$, NP and VSRs (NSs and
777 P19-HcPro-γb). (D) A *N. benthamiana* leaf infiltrated with a mixed Agrobacterium
778 culture carrying MR3$_{(-)eGFP}$, RdRp$_{opt}$, NP and VSRs (NSs and P19-HcPro-γb) and
779 was showing eGFP fluorescence at 5 dpi under an inverted fluorescence microscope.
780 Bar represents 200 μm.

781

782 **Fig. 2** RSV NP and RdRp$_{opt}$ are required for MR3$_{(-)eGFP}$ expression in *N. benthamiana*
783 leaves. (A) *N. benthamiana* leaves were infiltrated with mixed *Agrobacterium* cultures
784 carrying MR3$_{(-)eGFP}$+NSs+P19-HcPro-γb+Vec (empty vector),
785 MR3$_{(-)eGFP}$+NSs+P19-HcPro-γb+NP, MR3$_{(-)eGFP}$+NSs+P19-HcPro-γb+RdRp$_{opt}$, or

786 $MR3_{(-)eGFP}$+NSs+P19-HcPro-γb+$RdRp_{opt}$. The infiltrated leaves were examined and
787 photographed under an inverted fluorescence microscope at 5 dpi. Bars = 200 μm. (B)
788 Western blot analyses using the samples described in (A) and an NP or an eGFP
789 specific antibody. The ponceau S-stained Rubisco large subunit gel was used to show
790 sample loadings. (C) Northern blot analyses using the samples described in (A) and a
791 DIG-labeled sense- or an antisense-eGFP probe. The red and blue arrows indicate the
792 antigenomic and genomic RNA3 expressed the infiltrated leaves. The ethidium
793 bromide stained ribosomal RNA gel was used to show sample loadings.
794
795 **Fig. 3** Effects of VSRs on $pMR3_{(-)eGFP}$ expression. (A) *N. benthamiana* leaves were
796 infiltrated with mixed Agrobacterium cultures as indicated in the figure. The
797 infiltrated *N. benthamiana* leaves were harvested at 5 dpi, and examined and
798 photographed under an inverted fluorescence microscope. Bars = 200 μm. (B)
799 Western blot analyses using the samples described in (A), and an NP specific and an
800 eGFP specific antibodies, respectively. Proteins in the leaves shown in panel (A)
801 using NP and GFP-specific antibodies, respectively. The ponceau S-stained Rubisco
802 large subunit gel was used to show sample loadings.
803
804 **Fig. 4** Concentrations of NP and $RdRp_{opt}$ needed for the maximum expression
805 $MR3_{(-)eGFP}$. (A and B) *N. benthamiana* leaves were infiltrated with various mixed
806 Agrobacterium cultures as indicated in the figure. The concentration of
807 Agrobacterium cultures carrying NP or $RdRp_{opt}$ ranged from OD_{600} = 0 to 0.4. The

808 infiltrated leaves were harvested at 5 dpi, and examined and photographed under an
809 inverted fluorescence microscope. Bars = 200 μm. (C and D) Western blot analyses of
810 NP and eGFP expressions in the infiltrated leaves described in (A and B) using an NP
811 specific and an eGFP specific antibodies, respectively. The ponceau S-stained Rubisco
812 large subunit gel was used to show sample loadings.
813
814 **Fig. 5** Effect of RSV NSvc4 on eGFP expression from $MR3_{(-)eGFP}$ in cells. (A) *N.*
815 *benthamiana* leaves were infiltrated with various mixed Agrobacterium cultures as
816 described in the figure. The concentration of Agrobacterium culture carrying NSvc4
817 ranged from OD_{600} = 0 to 0.15. The infiltrated leaves were harvested at 5 dpi, and
818 examined and photographed under an inverted fluorescence microscope. Bars = 200
819 μm. (B) Western blot analyses using the infiltrated leaf samples described in (A), and
820 an NP specific and an eGFP specific antibodies, respectively. The ponceau S-stained
821 Rubisco large subunit gel was used to show sample loadings.
822
823 **Fig. 6** Construction and test of $RNA3_{(+)}$-based mini-replicon in *N. benthamiana*
824 leaves. (A) Schematics representing $RNA3_{(+)}$ and $MR3_{(+)eGFP}$ mini-replicons. The
825 $MR3_{(+)eGFP}$ mini-replicon was made by replacing the *NS3* gene in $RNA3_{(+)}$ with an
826 *eGFP* gene. Plus sign (+) and 3′ to 5′ designation represent the viral complementary
827 (antigenomic)-strand of RNA3. (B) *N. benthamiana* leaves were infiltrated with
828 various mixed Agrobacterium cultures as described in the figure. The infiltrated
829 leaves were observed at 5 dpi, and examined and photographed under an inverted

fluorescence microscope. Bars = 200 μm. (C) Schematics representing $MR3_{(-)eGFP}$ and $MR3_{(-)mCherry\&eGFP}$ mini-replicons. The $MR3_{(-)mCherry\&eGFP}$ mini-replicon was constructed by replacing the *NS3* gene with an *mCherry* gene. Minus sign (-) and 5′ to 3′ designation represent the viral (genomic)-strand of RNA3. (D) The infiltrated *N. benthamiana* leaves were harvested at 5 dpi, and examined and photographed under an inverted fluorescence microscope. Bars = 200 μm. (E) Northern blot analyses of RNA3 expressions from $RNA3_{(+)}$ in the infiltrated leaves as described in (C). After electrophoresis, the blots were probed with a DIG-labeled antisense and a sense RNA3 probes, respectively. The red and blue arrow heads indicate the RNA3 bands probed with DIG-labeled probes. The ethidium bromide stained ribosomal RNA (rRNA) gel was used to show sample loadings.

Fig. 7 Effect of NS3 on *eGFP* gene expression from the mini-replicons. (A and D) Schematics representing $MR3_{(-)eGFP}$ and its mutants. For $MR3_{(-)eGFP\Delta NS3}$, the *NS3* gene was deleted from $MR3_{(-)eGFP}$. For $MR3_{(-)eGFP\&NS3stop}$, a stop codon was introduced at the downstream of the start codon of the *NS3* gene in $pMR3_{(-)eGFP}$. For $MR3_{(-)eGFPMut1\ to\ 4}$ mutant mini-replicons, a quarter of the *NS3* gene in $MR3_{(-)eGFP}$ was deleted as shown in the figure. Minus sign (-) and 5′ to 3′ designation represent the viral (genomic)-strand of RNA3. (B and E) *N. benthamiana* leaves were infiltrated with various mixed Agrobacterium cultures as described in the figure. The infiltrated leaves were harvested at 5 dpi, and examined and photographed under an inverted fluorescence microscope. Bars = 200 μm. (C and F) Western blot analyses using the

leaf samples described in (B and E), and an NP specific and an eGFP specific antibodies, respectively. The ponceau S-stained Rubisco large subunit gels were used to show sample loadings. (G) Northern blot analyses of antigenomic and genomic RNA expressions from $MR3_{(-)eGFP}$ using a DIG-labeled antisense- and a sense-eGFP probe, respectively. The ethidium bromide-stained ribosomal RNA gel was used to show sample loadings.

Fig. 8 RNA secondary structures of the 3′-UTR, NS3 ORF and IGR region of RSV RNA3 segment. Secondary structure was predicted using the RNA fold web server (http://rna.tbi.univie.ac.at/cgi-bin/RNAWebSuite/RNAfold.cgi) based on thermodynamic prediction of minimal free energy (MFE). Red, black and blue arrows indicated the nucleotide positions in 3′-UTR, NS3 and IGR regions, respectively. Dotted boxes indicated that Hairpin 1 and 2 were formed by IGR, NS3 and 3′-UTR of RSV RNA3, respectively.

Fig. 9 Establishment of complete mini-replicon systems representing RSV RNA1, RNA2, RNA3, and RNA4 genomic RNA segments in *N. benthamiana* leaves. (A) Schematics representing $MR1_{(-)eGFP}$, $MR2_{(-)eGFP}$, and $MR4_{(-)eGFP}$ mini-replicons. The RSV *RdRp* gene in $MR1_{(-)eGFP}$, the *NSvc2* gene in $MR2_{(-)eGFP}$, and the *NSvc4* gene in $MR4_{(-)eGFP}$ were replaced with an *eGFP* gene to produce $MR1_{(-)eGFP}$, $MR2_{(-)eGFP}$, and $MR4_{(-)eGFP}$, respectively. Minus sign (-) and 5′ to 3′ designation represent the viral (genomic)-strand of RNA1, 2 and 4. (B) *N. benthamiana* leaves were infiltrated with

874 various mixed Agrobacterium cultures as described in the figures. The infiltrated leaf
875 tissues were harvested at 5 dpi, and examined and photographed under an inverted
876 fluorescence microscope. Bars = 200 μm.

877

878 **Table S1.** List of primers used in the study.

879

880 **Table S2.** The predicted intron splicing sites of wild-type RdRp gene.

881

882 **Table S3** Optimized RdRp gene sequence made in this study.

883

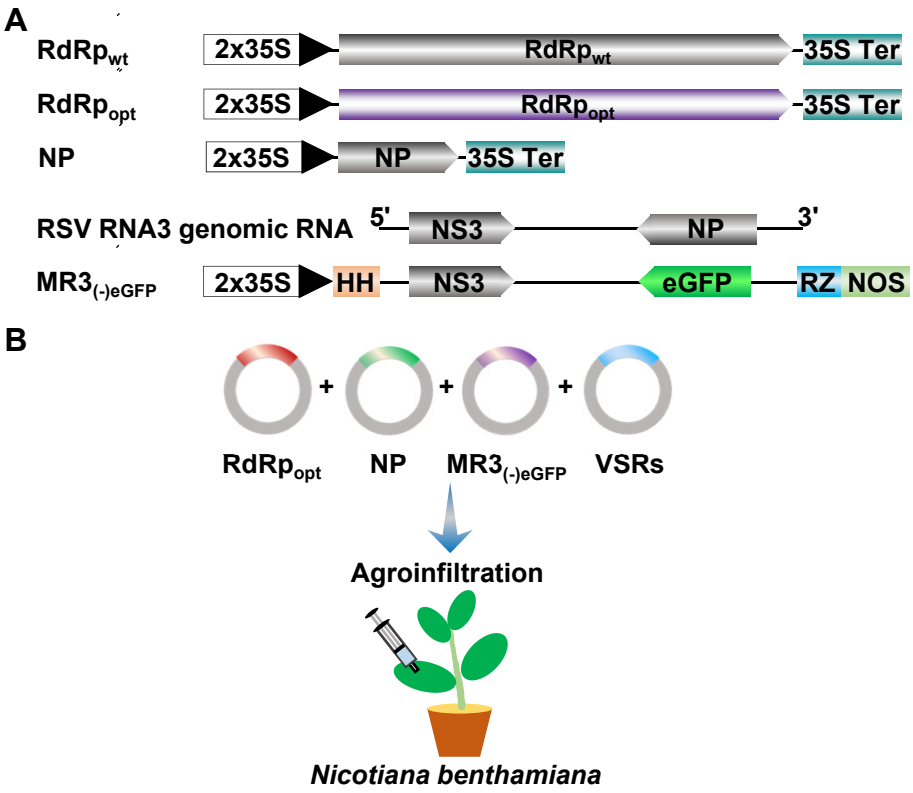

Fig. 1

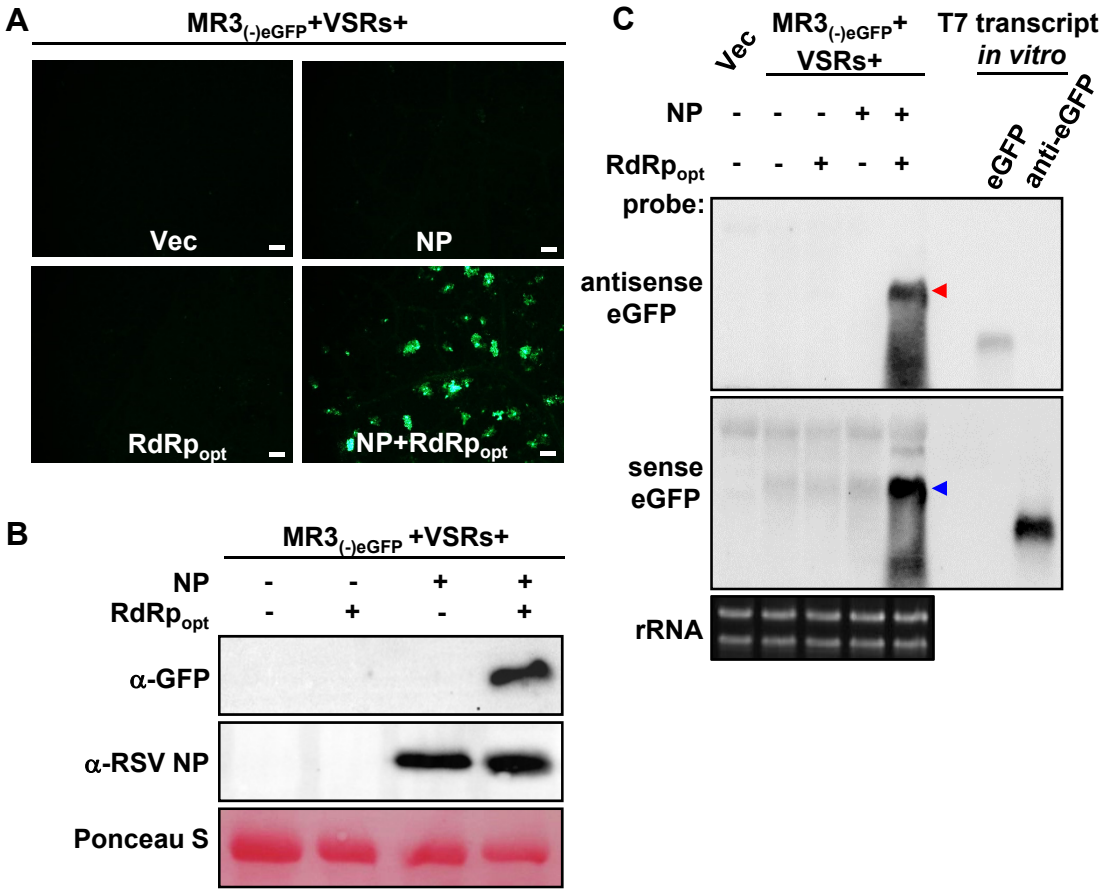

Fig. 2

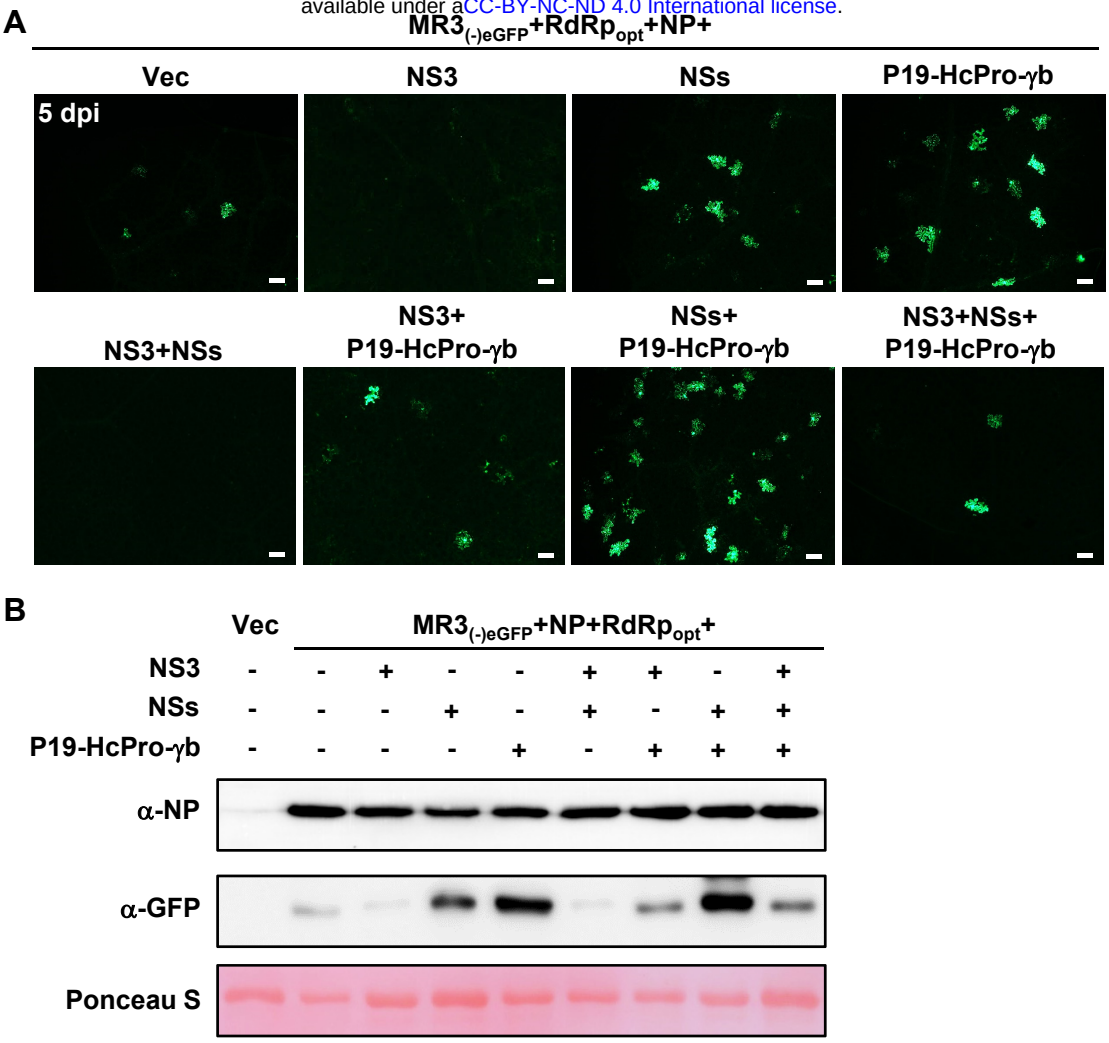

Fig. 3

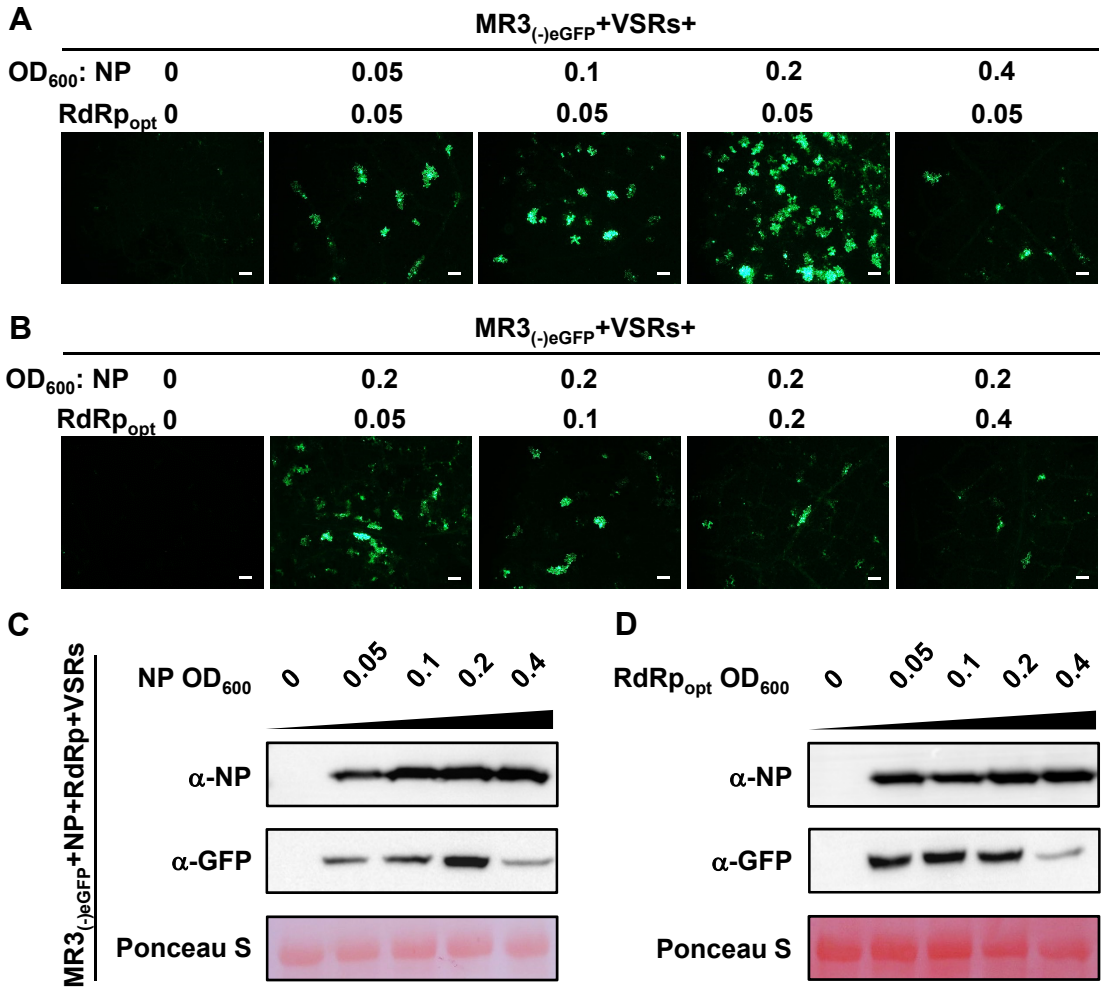

Fig. 4

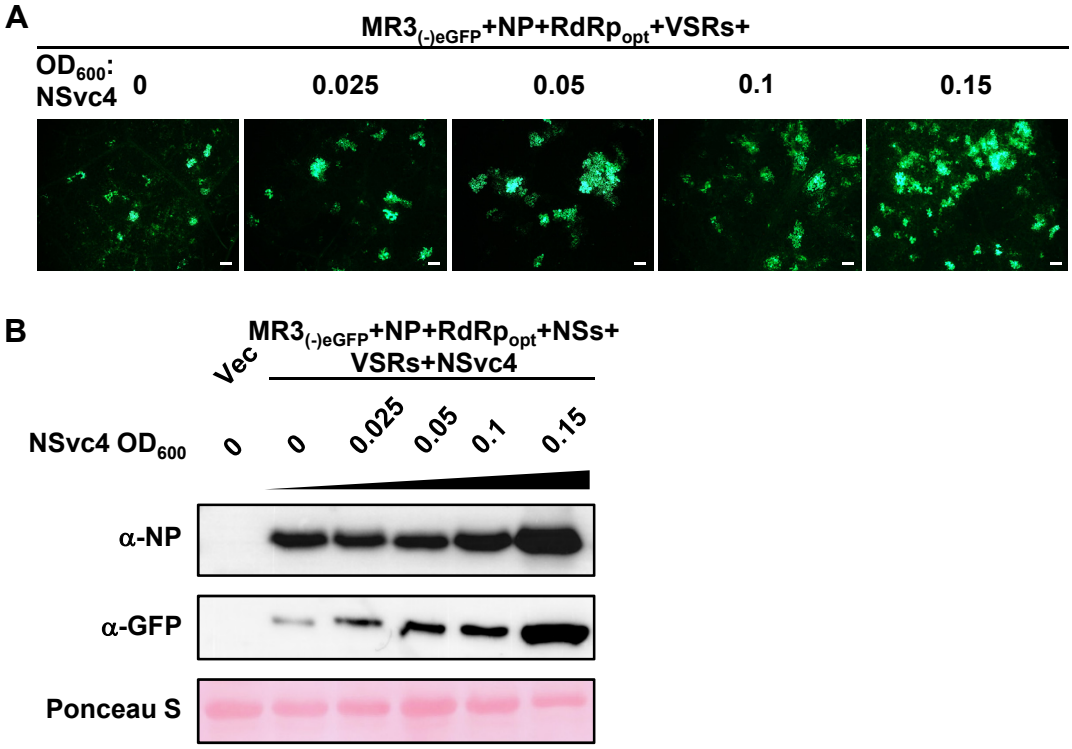

Fig. 5

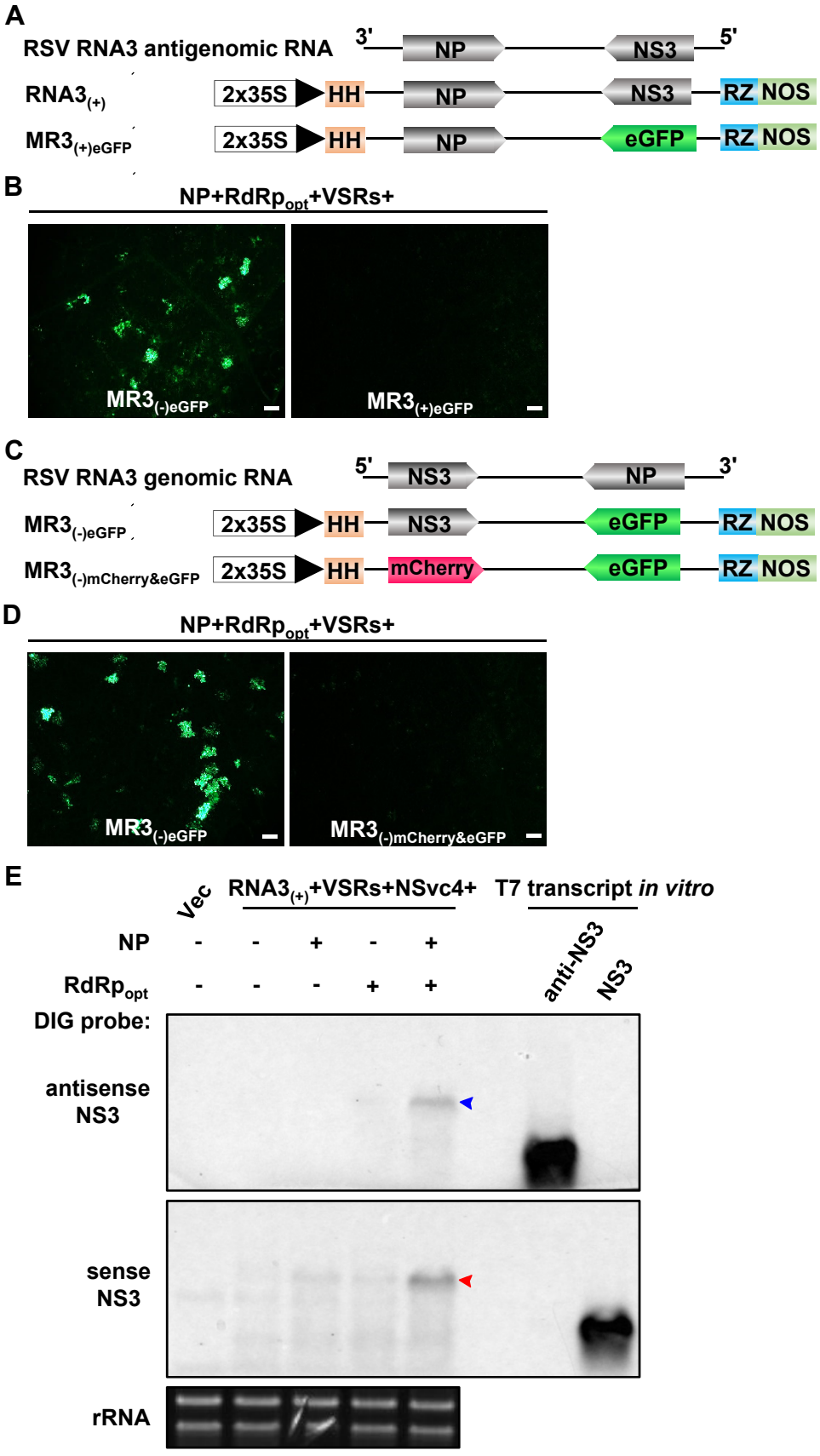

Fig. 6

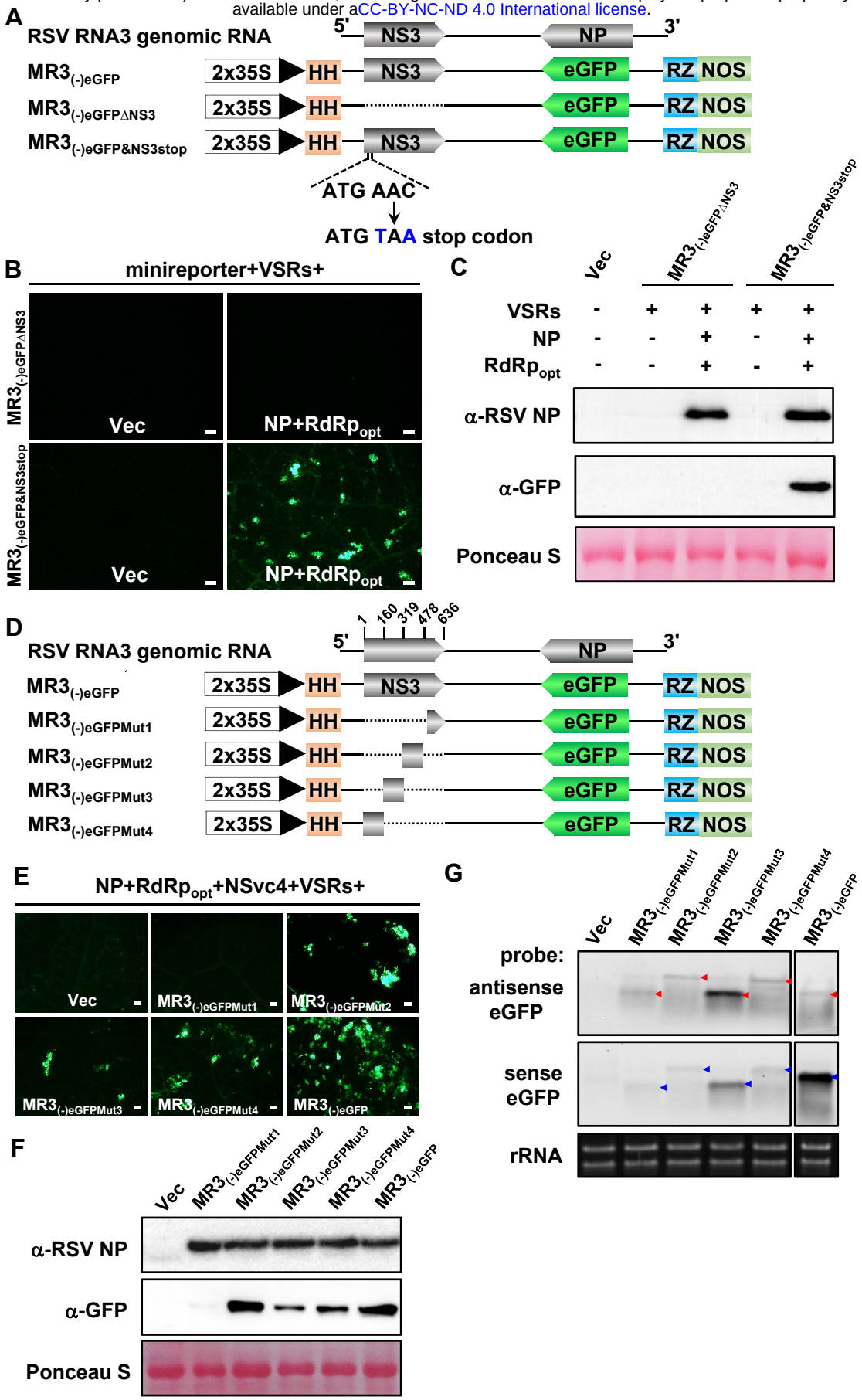

Fig. 7

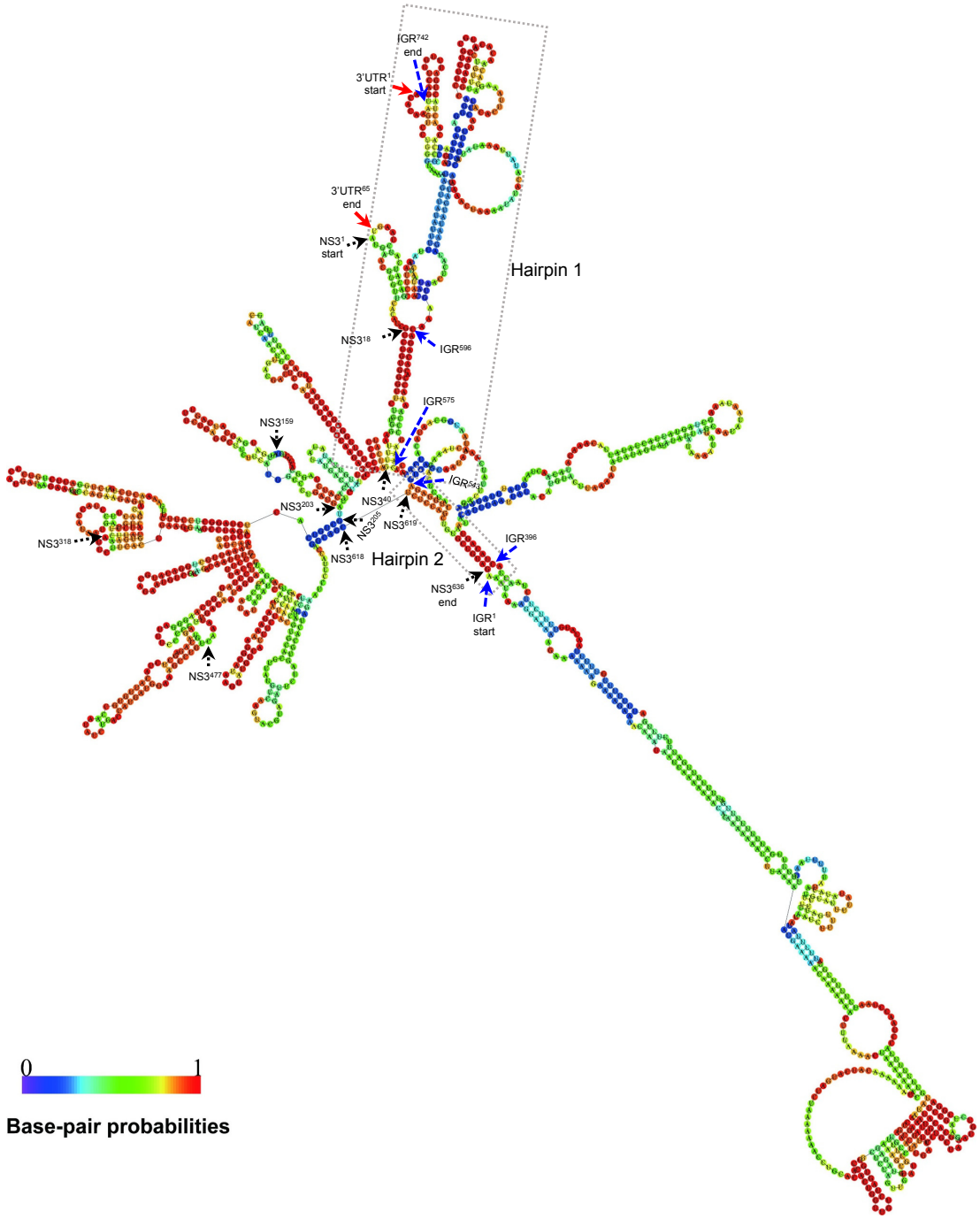

Fig. 8

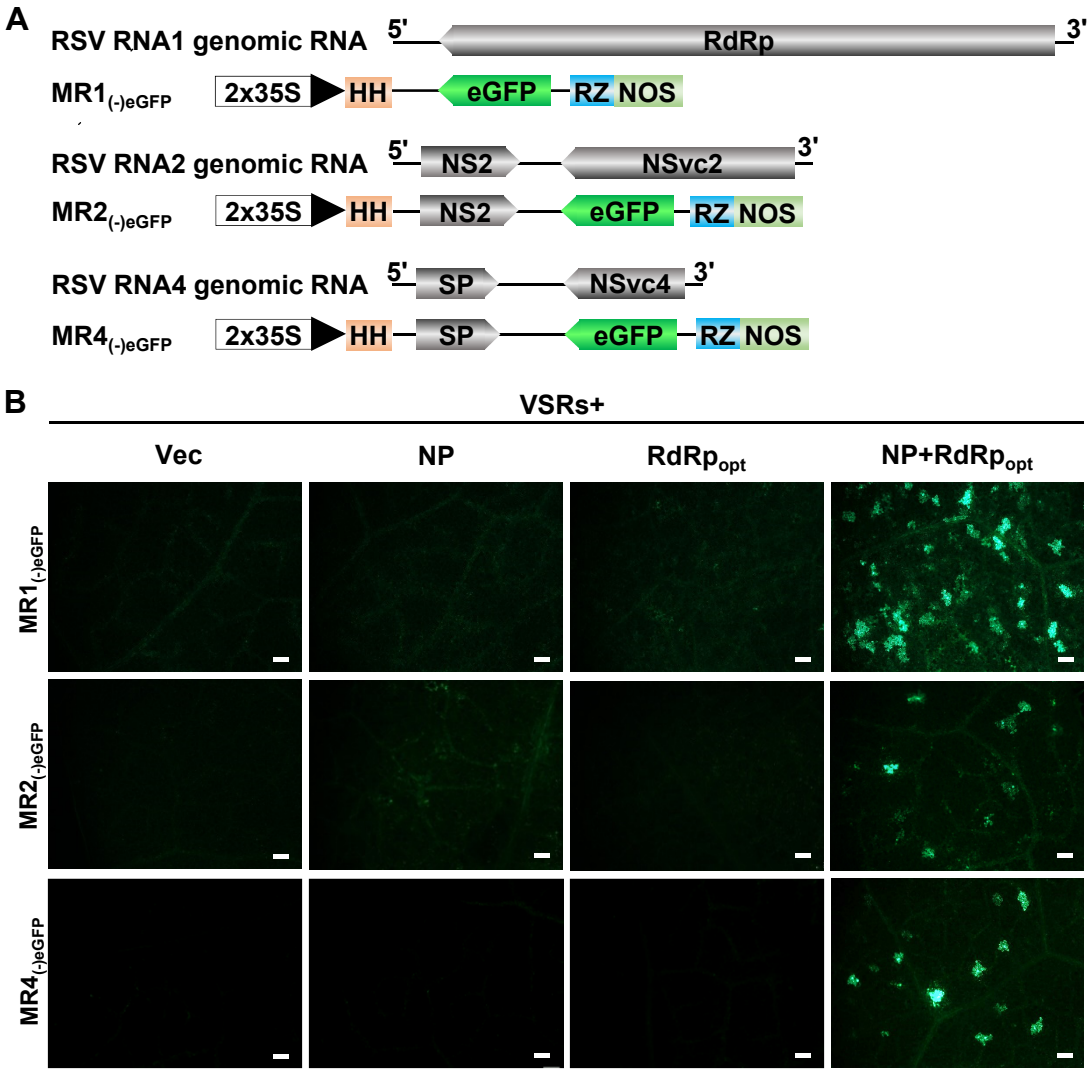

Fig. 9